Balamurugan
Journal of Engineering and Applied Science (2024) 71:142
https://doi.org/10.1186/s44147-024-00470-2

Journal of Engineering and Applied Science

RESEARCH Open Access

Investigation on the effect of laser surface texturing on the wettability of pure zinc substrate

Kannan Ganesa Balamurugan[1*]

*Correspondence:
gbmpondy@gmail.com

[1] Department of Mechanical Engineering, IFET College of Engineering, Tamil Nadu 605108, India

Abstract

Zinc finds a prominent metallic alternative for existing metallic bio-implant materials. Wettability significantly alters the corrosion resistance and cell adhesion of bio-metallic materials. The wettability of the metallic materials can be engineered by laser surface texturing (LST). In this work, nanosecond laser surface texturing experiments were conducted on the pure zinc substrate by varying the laser scan speed and texture pitch. Laser scan speeds were varied from 10 to 50 mm/s, and the texture pitch varied from 100 to 300 µm. A nanosecond 28 W Nd:YAG laser system was used with 1064 nm wavelength, repetition rate of 5 kHz, focal length of 234 mm, and pulse width of 2 ms. The white light interferometer (WLI) was utilized to explore the surface roughness of the textured samples, and the scanning electron microscope (SEM) was used to investigate the surface morphology. The results revealed that LST on pure zinc follows the Weinzel model which enhances the hydrophobic nature of its surface. Surface roughness plays a significant role in improving the hydrophobic nature of the LST zinc substrates.

Keywords: Laser surface texturing, Pure zinc, Bio-implant, Wettability

Introduction

Surface properties play a vital role in determining the life of the engineering products and critically should be monitored to avoid losses from wear and corrosion. Moreover, the engineering of surface topographies of materials can be utilized for various applications. The wettability of the materials can be altered by engineered surface topographies. The wettability nature of materials can be termed as hydrophobicity and hydrophilicity. Hydrophilicity is the nature of material surface with the affinity to water and maximizes the contact with the water. However, in case of hydrophobicity, the nature of the material surface repels the water by minimizing the contact with it. The hydrophilic surfaces can be utilized for anti-fogging applications, biomedical applications, etc. Likewise, the hydrophobic surfaces can be utilized for wear improvement, corrosion improvement, self-cleaning applications, etc. The superhydrophilic and superhydrophobic surfaces are the extreme wettability conditions and can be engineered by various methods for different applications [1]. Surface texturing is a novel approach to engineering the material

surfaces to become superhydrophobic and superhydrophilic. Electrochemical deposition [2], anodic oxidation [3, 4], galvanic exchange reaction [5], electrochemical etching [6], sol–gel route [7], template method [8], expanding plasma arc [9], and sintering process [10] methods have been applied to fabricate textures on the material surfaces. However, these methods have their own limitations like adverse environmental impacts and low efficiency in texture formation [11]. To overcome these constraints, currently, a laser-based surface texturing technique has been adopted [12, 13]. In the laser texturing process, a high-intensity laser beam irradiates the material surface wherever it is exposed. This irradiation creates micro dimples and micro grooves as per the exposing nature of the laser beam. Several researchers have attempted laser surface texturing (LST) on different kinds of materials, especially on metallic materials. Keitzig et al. [14] applied the laser texturing technique to create some double-scale roughness surface textures on different alloys of metals using a femtosecond laser. The initial textured surface favoured the superhydrophilic nature, and after the extended time period, superhydrophilic surfaces were converted to superhydrophobic. Li et al. [15] attempted to fabricate stable superhydrophilic and superhydrophobic surfaces on the titanium plates by superficial femtosecond laser scanning and silanization modification. As a result of laser texturing among two mutually perpendicular directions, micrometer spikes, and nanometer ripples were formed on the Ti surface. Textured surfaces show the superhydrophilic before silanization. However, after silanization, textured surfaces exhibited higher superhydrophobic. Yang et al. [16] had textured the Inconel 718 by a nanosecond laser. Different kinds of patterns like lines, grids, and spots were textured on the Inconel 718. Initial textured surfaces show superhydrophilic nature then transformed to superhydrophobic nature over 20 days. Among the metallic materials, bio-metallic materials make a significant focus due to their crucial biomedical applications. Usually, the performance of metallic biomaterials can be improved by laser microprocessing. Recently, zinc and zinc-based alloys have been identified as prominent biodegradable materials for biomedical applications [17–19]. A lack of LST works has been reported on zinc substrates. Therefore, in this work, laser surface texturing was attempted to texture on a pure zinc substrate. The effect of the laser surface texturing on the texture formation and wettability was investigated.

Experimental

As cast zinc substrate was machined to the sample size of $50 \times 50 \times 5$ mm. Sample surfaces were polished with different kinds of grade sheets to ensure flatness and cleaned with alcohol. The selected laser texturing area was 30×30 mm. A single groove texture was selected for patterning. LST parameters are shown in Table 1. A nanosecond 28 W Nd:YAG laser system was used with a 1064 nm wavelength, repetition rate of 5 kHz, focal length of 234 mm, and pulse width of 2 ms. LST was performed with predetermined process parameters. Textured samples were subjected to microstructural examination to analyse the nature of texture formation by scanning electron microscope (SEM), and the elemental formation in the textured surfaces was examined by electric discharge spectrometry (EDS). Textured samples were cleaned with ethanol, and sample sizes of 10×10 mm were prepared to accommodate them in the SEM machine. The 2D topography, the 3D topography, and the surface roughness were evaluated by white light

Table 1 LST parameters

Texture type	Texture pitch in µm	Laser beam scan speed in mm/s
Type-1	100	10
Type-2	100	50
Type-3	300	10
Type-4	300	50

interferometer (WLI). Textured sample surfaces were scanned by the white light emitted by the WLI, and the corresponding images were created. Using Gydwin software, 2D and 3D topographies and surface roughness were generated. The wettability of the textured samples was investigated through a contact angle meter (SmartDropSDLab-200TEZD, FemtoFab, Korea). A total of 10 µL of a water droplet was poured through a contact angle meter needle on the specific textured surface. The image of the drop was captured through a camera and analysed with software.

Results and discussion

Effect of laser scanning speed on the morphology of textured zinc substrates

Figure 1 shows the SEM images of the morphology of zinc surface textured with 100 µm pitch and 10 mm/s scan speed. The low magnification morphology (Fig. 1a) shows that parallel grooves with vague boundaries were fabricated by the nanosecond laser irradiation. Higher magnification of the texture (Fig. 1b) shows the high density of recast materials. These recast materials fill the groove cavities, and the groove profile has been distorted.

Figure 2 shows the SEM images of the morphology of zinc surface textured with 100 µm pitch and 50 mm/s scan speed. Low magnification morphology (Fig. 2a) shows the parallel groove textures with shallow depth. Minimal recast materials around and between the textures were observed. Higher magnification images (Fig. 2b) show the minimal recast materials in the groove cavity.

Figure 3 shows the SEM images of the morphology of zinc surface textured with 300 µm pitch and 10 mm/s scan speed. Lower magnification SEM images (Fig. 3a) show a distinct boundary between each texture. These distinct boundaries resulted from the increased pitch between them. Recast materials were splashed and settled around the boundaries of the textured grooves. Moreover, the higher magnification SEM image of the textured groove (Fig. 3b) clearly shows the dominance of these recast materials inside the grooved cavities.

Figure 4 shows the SEM images of the morphology of zinc surface textured with 300 µm pitch and 50 mm/s scan speed. Lower magnification SEM images (Fig. 4a) show distinct boundaries due to increased pitch between the textures. Higher magnification SEM image (Fig. 4b) shows a cavity of a textured groove with minimal recast materials.

Figure 5 indicates the 2D surface topography of a single groove cavity of the texture, detected by a white light interferometer. 2D topographies resemble the nature of texture groove cavities. Texture cavities were widening from texture type-1 to texture type-4.

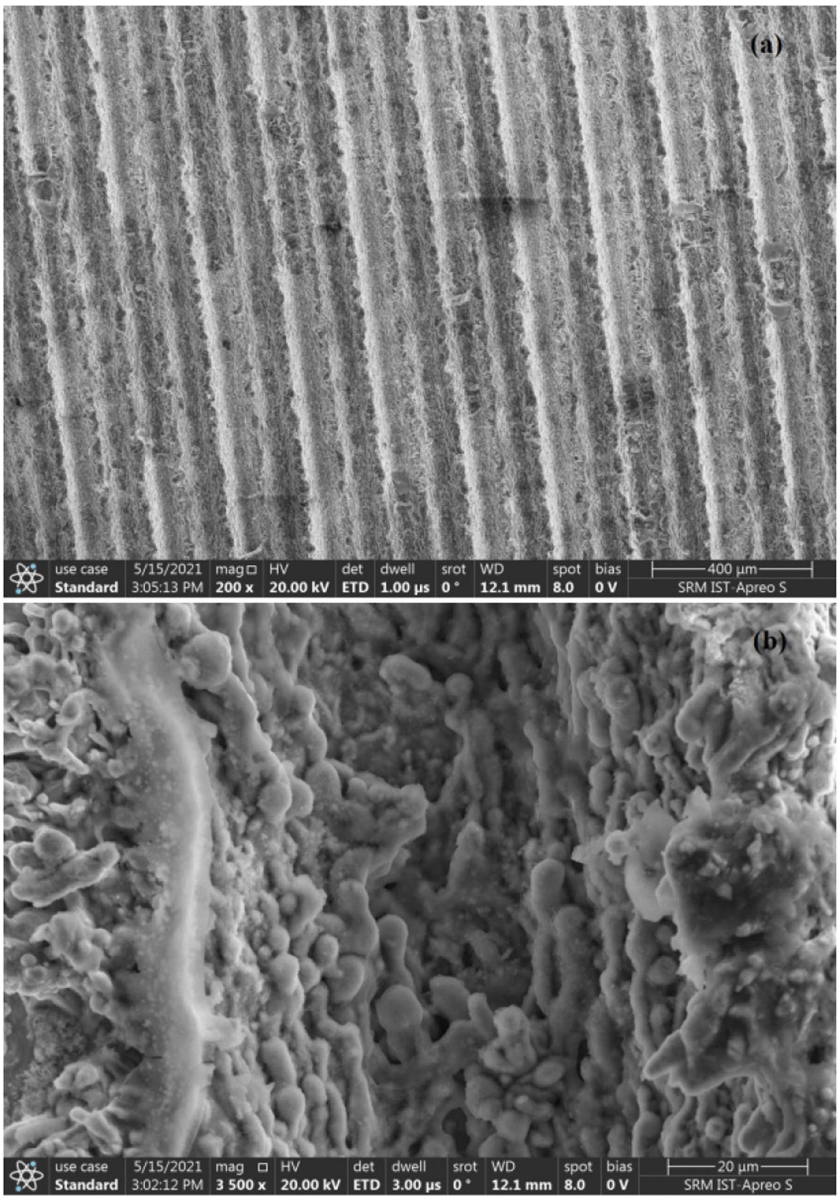

Fig. 1 SEM images of zinc surface textured with 100 µm pitch and 10 mm/s scan speed. **a** Low magnification textured surface. **b** High magnification textured surface

Similarly, the texture cavity depths were varying from texture type-1 to texture type-4. The average cavity depth and length of texture types are presented in Table 2.

Table data indicate that higher cavity depth and length were observed in Texture type-1. Similarly, higher cavity depth was observed in Texture type-3. A drastic reduction in texture depths was observed in type-2 and type-4, respectively. However, cavity lengths were gradually reduced from type-1 to type-4.

3D topographies show the nature of the texture grooves. Clear texture groove formations were observed in texture type-1 and texture type-3 (Fig. 6).

Surface roughness Rz of the textured zinc substrates was evaluated from their surface topographies data. Figure 7 shows the surface roughness of the textured zinc substrates.

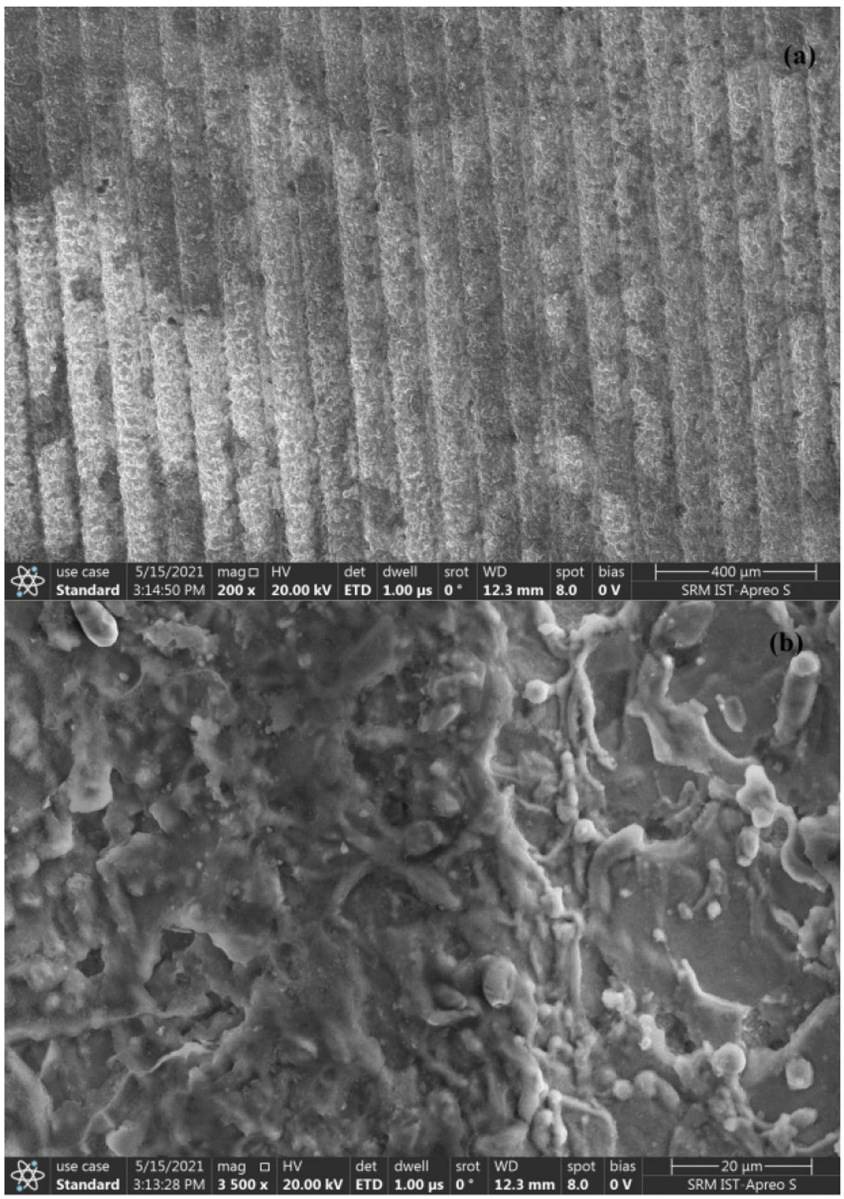

Fig. 2 SEM images of zinc surface textured with 100 µm pitch and 50 mm/s scan speed. **a** Low magnification textured surface. **b** High magnification textured surface

The result indicates that a higher surface roughness of 213.1 Rz has been observed in texture-1, and the next higher Rz has been observed in texture type-3 (160.9 Rz). The lowest surface roughness of 58.72 Rz was observed in texture type-2 and the texture type-4 shows the Rz of 62.45.

When a high-intensity laser beam interacts with a material surface, it irradiates the surface of the material and removes the materials by melting and vaporization [20]. Laser ablation is the function of the laser power intensity. The laser power intensity is influenced by the laser power to concentrate its beam into a prescribed area. Increased power intensity increases the material removal. In this research, laser power was kept constant to investigate the effect of laser scanning speed on the texture morphology. The

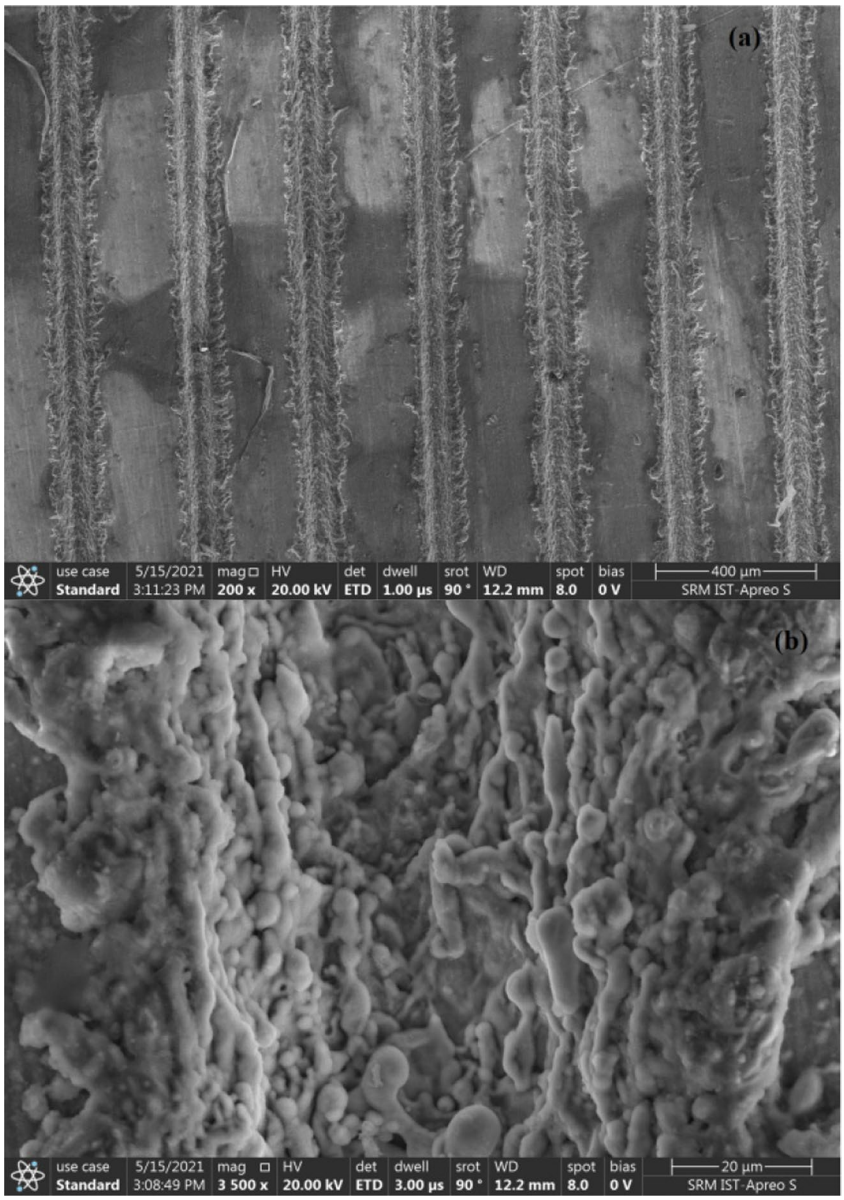

Fig. 3 SEM images of zinc surface textured with 300 µm pitch and 10 mm/s scan speed. **a** Low magnification textured surface. **b** High magnification textured surface

laser scanning speed is the constant movement of a laser beam on the material surface to process it along a prescribed length. A laser beam irradiates the contacted surface along the path. The irradiation melts and vaporises the materials forming a cavity along the length of the laser beam travel. Material removal and crater depth depend on the laser beam exposing period on the prescribed spot of the material. The scanning speed of the laser governs the exposing period. An increase in the exposing period of the laser beam increases the concentration of the laser energy in the specific spot of the material. Thermal gradients are increased at that specific spot due to the absorption of higher laser energy. Intense heat input melts the material and further starts to vaporise it. When the laser beam moves to the next spot, the previous spot maintains the molten state and

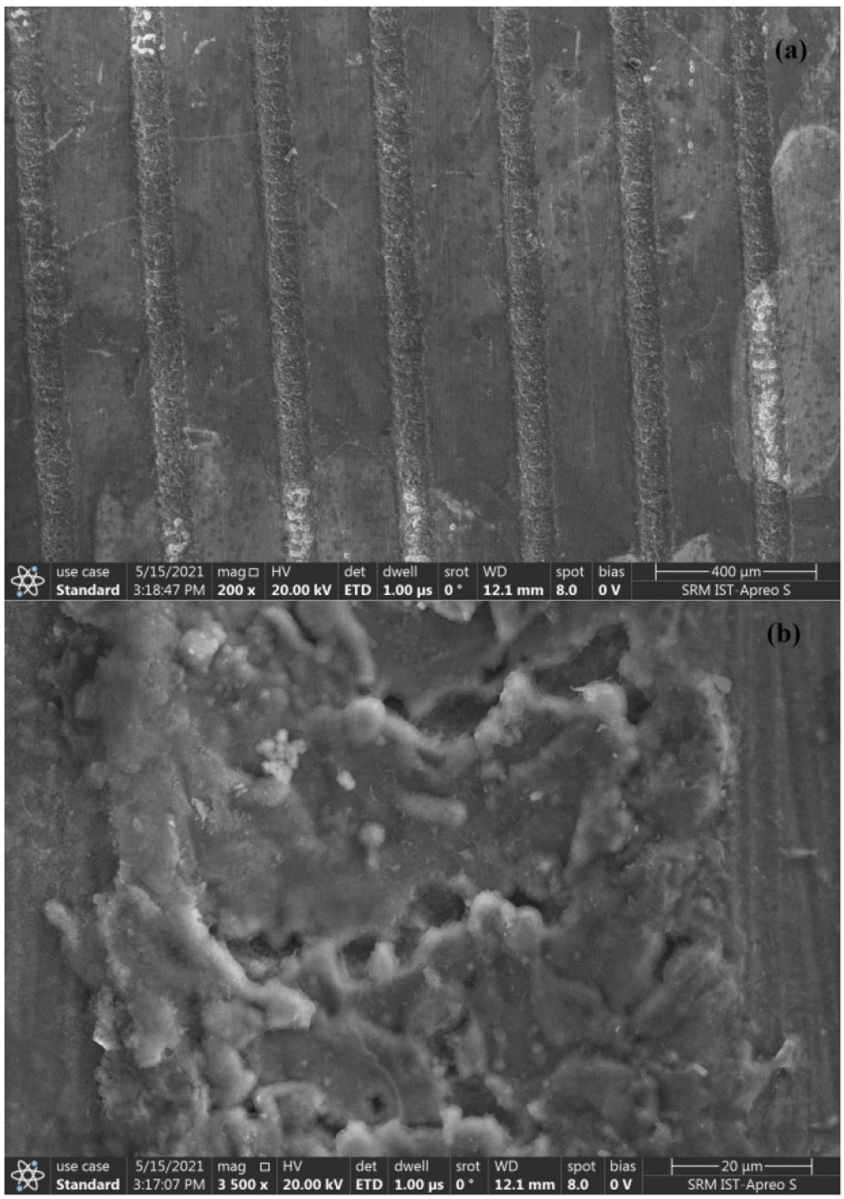

Fig. 4 SEM images of zinc surface textured with 300 µm pitch and 50 mm/s scan speed. **a** Low magnification textured surface. **b** High magnification textured surface

the plume. The plume is the vaporised state of the material irradiated by laser energy. When the spot receives the laser energy supply, the molten state and plume start a rapid solidification. This rapid solidification resulted in the formation of recast materials along and around the textured groove. However, the lower exposing period has restricted the formation of recast materials and induced micro cracks. These micro-cracks form surface patches along the processed length. The lower exposing period supplied low laser energy, and rapid movement of the laser beam induced a non-uniform solidification which resulted in micro cracking. A lower scan speed facilitates a higher interaction period, and a higher scan speed facilitates a lower interaction period. Therefore, 10 mm/s scan speed textures showed a higher density of recast materials than 50 mm/s

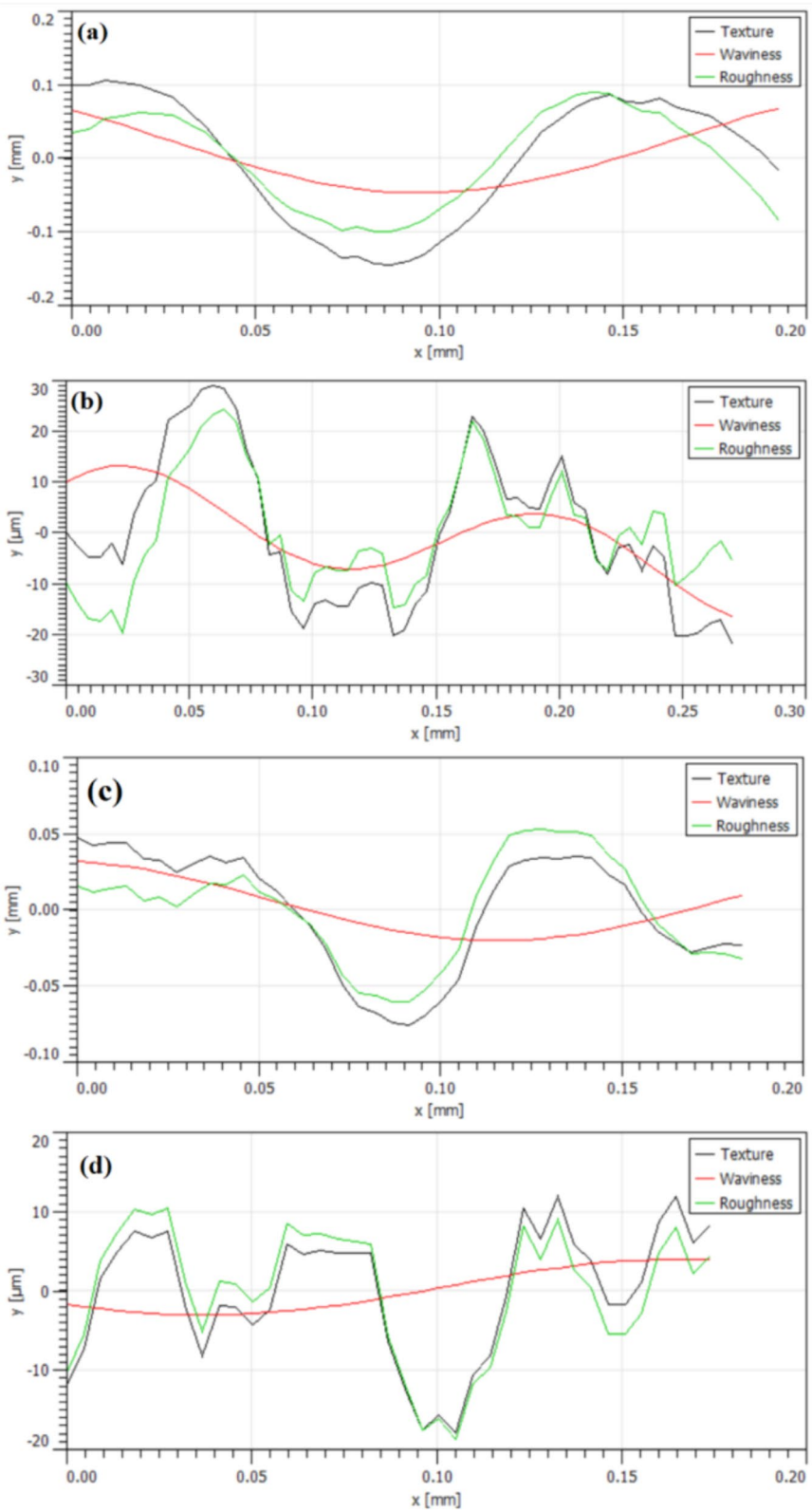

Fig. 5 2D topographies of textured Zinc surfaces. **a** 100 µm–10 mm/s. **b** 100 µm–50 mm/s. **c** 300 µm–10 mm/s. **d** 300 µm–50 mm/s

Table 2 Dimensions of the texture types

Texture type	Cavity depth in µm	Cavity length in µm
Type-1	244.7	109.3
Type-2	43.4	101.2
Type-3	109.5	73.4
Type-4	22.6	41.3

scan speed textures. The laser energy absorption of zinc is high due to its lower melting point which vaporise the material rapidly and forms the deeper craters. Therefore, deeper grooves were observed at 10 mm/s scan speed. Therefore, the texture type-1 and type-3 grooves showed higher depth cavities (refer to Table 1.) compared to the texture types 2 and 3. The 2D topographies (refer to Fig. 5a and c) of type-1 and type-3 textures showed a smooth profile of the cavities compared with the cavities of the texture type-2 and type-4 (refer to Fig. 5b and d). The 3D topographies of the type-1 and type-3 textures (refer to Fig. 6a and c) showed distinct patterns due to their sufficient cavities depth. Nature surfaces can be evaluated through their surface roughness. LST significantly affects the surface roughness of the metallic materials. The intensity of the surface irregularities determines the surface roughness ranges of the substrates. In LST substrates, the intensity of surface irregularities is governed by the recast materials and the textured cavities. High intensity of recast materials increases the surface irregularities and thus increases the surface roughness. Therefore, texture type-1 and texture type-3 show high surface roughness with high intensity of recast materials. Moreover, higher texture depth improves the surface roughness which can be advocated by the texture type-1 and type-3.

Effect of laser scanning speed on the wettability of the zinc substrate

Figure 8 represents the water contact angle of the LST zinc substrates. Texture type-1 shows the higher water contact angle of 130°, and the next higher water contact angle was observed in texture type-3 (127°). Lower water contact angles were observed in texture types 2 (118°) and 4 (123°).

The water contact angle is a common technique to measure the wettability of the surfaces. Major wettability mechanisms can be explained by either Wenzel or Cassie–Baxter models. The Wenzel model describes that surface roughness improves the nature of the wettability caused by the surface chemistry, which means the surface roughness improves the hydrophobicity of a natural hydrophobic surface. However, the Cassie–Baxter model suggests that the surface roughness entirely changes the wettability nature of the material surface. For example, as per the Cassie–Baxter model, a hydrophilic surface changes to hydrophobic. This indicates that material surface chemistry and roughness play a major role in determining the wettability characteristics of a material. The WCA measurement on the plain zinc substrate is hydrophobic. Low surface energy may be attributed to the hydrophobic nature of the zinc surface. The wettability results of the textured zinc surfaces showed an improved hydrophobicity due to increased surface

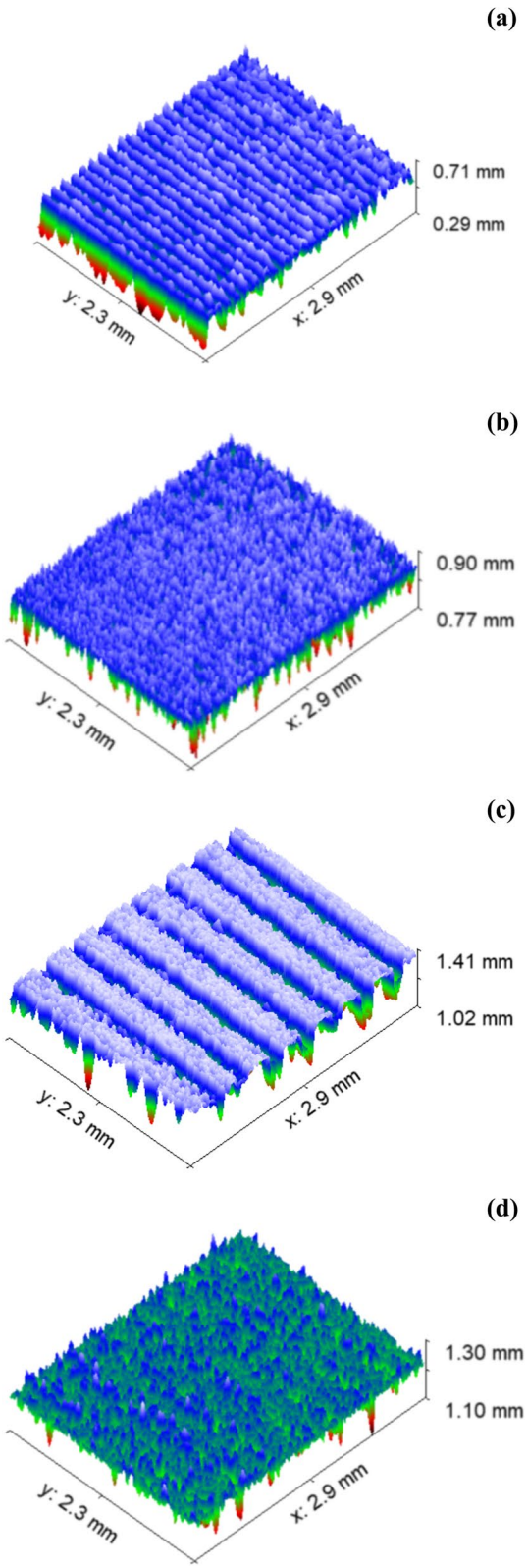

Fig. 6 3D topographies of textured Zinc surfaces. **a** 100 µm–10 mm/s. **b** 100 µm–50 mm/s. **c** 300 µm–10 mm/s. **d** 300 µm–50 mm/s

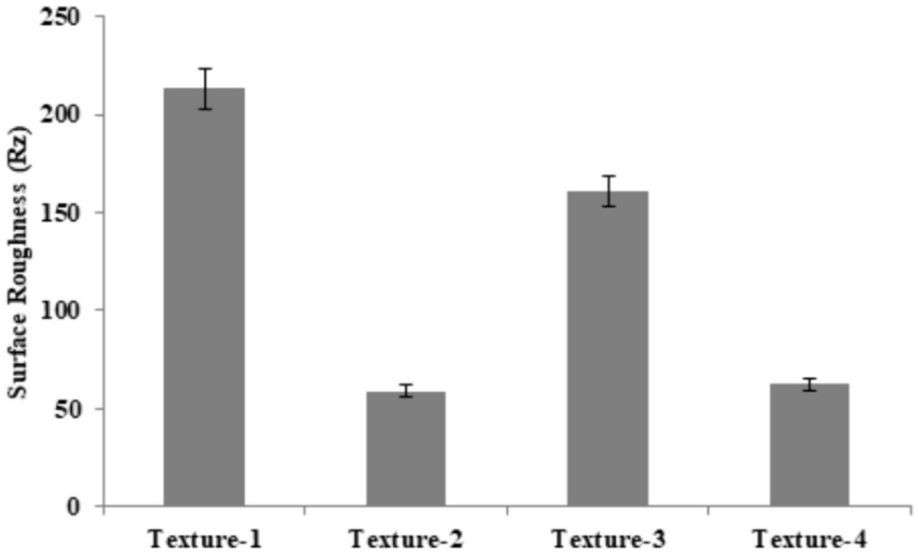

Fig. 7 Surface roughness of the textured zinc substrates

roughness by laser texturing. Hence, the surface textured zinc surfaces obey the Wenzel model of wettability. In this work, the wettability has been primarily governed by the surface roughness rather than the surface chemistry of the material. Texture types 1 and 3 show higher WCA with higher surface roughness compared to other texture types. The spikes of the rough surfaces hold the water droplets, and the air gap that exists between the spikes restricts the penetration of droplets further. Entrapped air between the droplet and spikes provides a cushioning effect to the droplet. This cushioning effect causes the resistance to the movement of the droplet. Thus, the lower laser scan speed and higher texture density (that is the lower pitch of the textures) increase the surface roughness which results in higher WCA. In the lower texture density case, the chances of landing of droplets on the pitch area rather than textured areas may reduce the WCA due to low surface roughness. Therefore, laser scan speed and pitch influence the wettability of the zinc surface.

Conclusions

In this work, the effect of LST parameters like scan speed and pitch on the texture formation and surface roughness on the commercially pure zinc substrate has been investigated. The following conclusions were arrived from this investigation.

1. Lower laser scan speed increases the texture cavity depth due to a higher exposure period with the zinc substrate. Therefore, the textures fabricated at 10 mm/s scan speed formed a higher cavity depth.
2. The lower scan speed increases the intensity of the recast materials which results in increased surface roughness.
3. Similarly, texture pitch also influences the agglomeration of the recast materials which affects the surface roughness. Minimal pitch value increases the agglomeration of the recast materials, and thus, the increase in surface roughness has resulted.

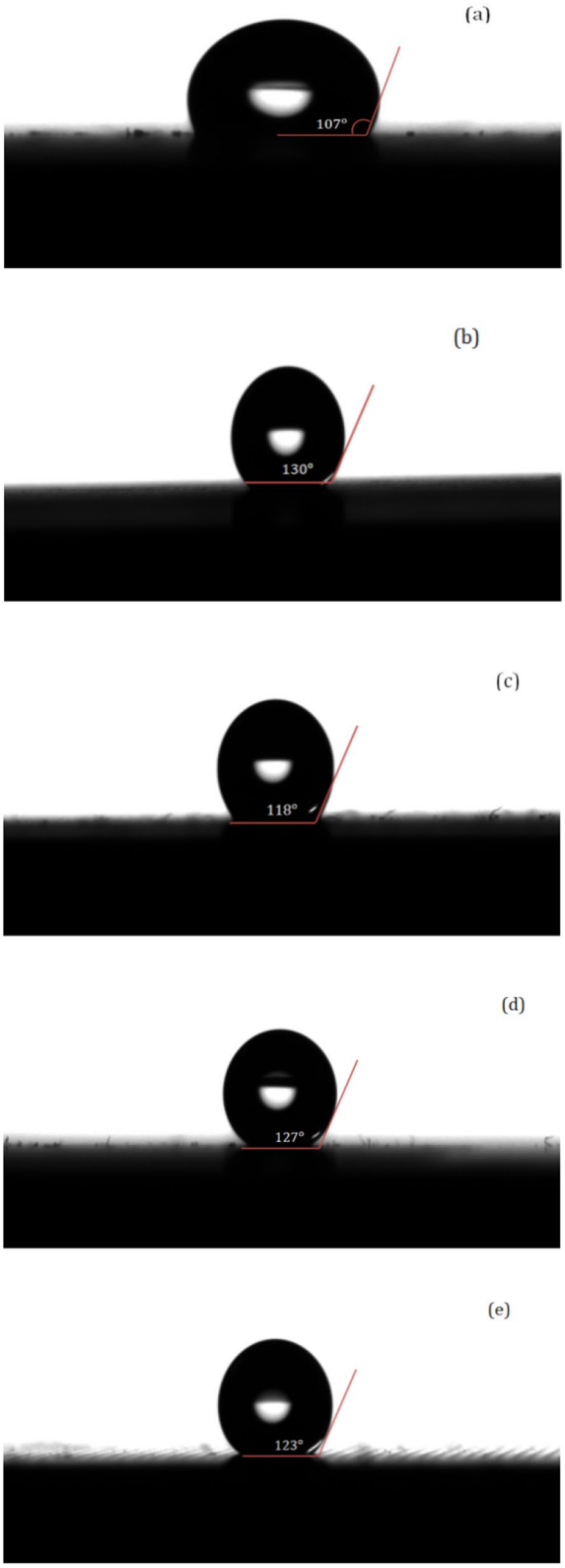

Fig. 8 Water contact angle of LST zinc substrates. **a** Base materials. **b** 100 µm–10 mm/s. **c** 100 µm–50 mm/s. **d** 300 µm–10 mm/s. **e** 300 µm–50 mm/s

4. Untreated pure zinc substrate exhibits a hydrophobic surface. LST zinc substrate follows the Wenzel model by improving the water contact angle. Thus, the LST zinc substrate transforms into superhydrophobic.
5. Fabricated textures hold the water droplet during its deposition and prevent its penetration into the surface by providing resistance by entrapping the air between them and inside their cavities.

Abbreviations

LST	Laser surface texturing
WLI	Wight light interferometer
SEM	Scanning electron microscope
µm	Micrometer
WCA	Water contact angle
Nd:YAG	Neodymium-doped yttrium aluminum garnet
W	Watts
2D	Two dimensional
3D	Three dimensional

Acknowledgements
Not applicable.

Author's contributions
Kannan Ganesa Balamurugan: experiment design, execution, analysis, and drafting.

Funding
Not applicable.

Availability of data and material
Data availability upon request.

Declarations

Competing interests
The author declares that he has no competing interests.

Received: 2 May 2023 Accepted: 11 June 2024
Published online: 22 June 2024

References

1. Du Q, Ai J, Qin Z, Liu J, Zeng X (2018) Fabrication of superhydrophobic/superhydrophilic patterns on polyimide surface by ultraviolet laser direct texturing. J Mater Process Tech 251:188–196
2. Wang J, Li A, Chen H, Chen D (2011) Synthesis of biomimetic superhydrophobic surface through electrochemical deposition on porous alumina. J Bionic Eng 8:122–128
3. Zhang F, Chen S, Dong L, Lei Y, Liu T, Yin Y (2011) Preparation of superhydrophobic films on titanium as effective corrosion barriers. Appl Surf Sci 257:2587–2591
4. Liang J, Liu K, Wang D, Li H, Li P, Li S, Su S, Xu S, Luo Y (2015) Facile fabrication of superhydrophilic/superhydrophobic surface on titanium substrate by single-step anodization and fluorination. Appl Surf Sci 338:126–136
5. Cao Z, Xiao D, Kang L, Wang Z, Zhang S, Ma Y, Fu H, Yao J (2008) Superhydrophobic pure silver surface with flower-like structures by a facile galvanic exchange reaction with [Ag(NH3)2]OH. Chem Commun 23:2692–2694
6. Lu Y, Xu WJ, Song JL, Liu X, Xing YJ, Sun J (2012) Preparation of superhydrophobic titanium surfaces via electrochemical etching and fluorosilane modification. Appl Surf Sci 263:297–301
7. Caldarelli A, Raimondo M, Veronesi F, Boveri G, Guarini G (2015) Sol–gel route for the building up of superhydrophobic nanostructured hybrid-coatings on copper surfaces. Surf Coat Technol 276:408–415
8. Kang C, Lu H, Yuan S, Hong D, Yan K, Liang B (2012) Superhydrophilicity/superhydrophobicity of nickel micro-arrays fabricated by electroless deposition on an etched porous aluminum template. Chem Eng J 203:1–8
9. Satyaprasad A, Jain V, Nema SK (2007) Deposition of superhydrophobic nanostructured Teflon-like coating using expanding plasma arc. Appl Surf Sci 253:5462–5466
10. Hu J, Yuan W, Yan Z, Zhou B, Tang Y, Li Z (2015) Fabricating an enhanced stable superhydrophobic surface on copper plates by introducing a sintering process. Appl Surf Sci 355:145–152
11. Isimjan TT, Wang T, Rohani S (2012) A novel method to prepare superhydrophobic, UV resistance and anti-corrosion steel surface. Chem Eng J 210:182–187

12. Ta VD, Dunn A, Wasley TJ, Li J, Kay RW, Stringer J, Smith PJ, Esenturk E, Connaughton C, Shephard JD (2016) Laser textured superhydrophobic surfaces and their applications for homogeneous spot deposition. Appl Surf Sci 365:153–159
13. Ta VD, Dunn A, Wasley TJ, Kay RW, Stringer J, Smith PJ, Connaughton C, Shephard JD (2015) Nanosecond laser textured superhydrophobic metallic surfaces and their chemical sensing applications. Appl Surf Sci 357:248–254
14. Kietzig AM, Hatzikiriakos SG, Englezos P (2009) Patterned superhydrophobic metallic surfaces. Langmuir 25(8):4821–4827
15. Li BJ, Li H, Huang LJ, Ren NF, Kong X (2016) Femtosecond pulsed laser textured titanium surfaces with stable superhydrophilicity and superhydrophobicity. Appl Surf Sci 389:585–593
16. Yang Z, Tian YL, Yang CJ, Wang FJ, Liu XP (2017) Modification of wetting property of Inconel 718 surface by nanosecond laser texturing. Appl Surf Sci 414:313–324
17. Bowen PK, Shearier ER, Zhao S, Guillory RJ, Zhao F, Goldman J, Drelich JW (2016) Biodegradable metals for cardiovascular stents: from clinical concerns to recent Zn-alloys. Ad Healthc Mater 5:1121–1140
18. Venezuela J, Dargusch MS (2019) The influence of alloying and fabrication techniques on the mechanical properties, biodegradability and biocompatibility of zinc: a comprehensive review. Acta Biomater 87:1–40
19. Dambatta MS, Kurniawan D, Izman S, Yahaya B, Hermawan H (2015) Review on Zn based alloys as potential biodegradable medical devices materials. Appl Mech Mater 776:277–281
20. Riveiro A, Maçon AL, del Val J, Comesaña R, Pou J (2018) Laser surface texturing of polymers for biomedical applications. Front Phys 6:16

Publisher's Note